Physics of Fluids

Explicit series solutions for supersonic flat-plate boundary layer flows

Cite as: Phys. Fluids **34**, 073607 (2022); https://doi.org/10.1063/5.0099475
Submitted: 17 May 2022 • Accepted: 24 June 2022 • Accepted Manuscript Online: 27 June 2022 • Published Online: 14 July 2022

Ling Liu (刘玲), Jing Li (李靖) and Shijun Liao (廖世俊)

View Online Export Citation CrossMark

ARTICLES YOU MAY BE INTERESTED IN

Control of supersonic compression corner flow using a plasma actuator
Physics of Fluids **34**, 073605 (2022); https://doi.org/10.1063/5.0096511

Characteristics of boundary-layer transition driven by diverse streamwise vortices
Physics of Fluids **34**, 074113 (2022); https://doi.org/10.1063/5.0098544

Pore-scale study of the effect of bifurcated fracture on spontaneous imbibition in heterogeneous porous media
Physics of Fluids **34**, 072003 (2022); https://doi.org/10.1063/5.0095553

APL Machine Learning
Open, quality research for the networking communities
Now Open for Submissions
LEARN MORE

AIP Publishing

© 2022 Author(s).

Physics of Fluids ARTICLE scitation.org/journal/phf

Explicit series solutions for supersonic flat-plate boundary layer flows

Cite as: Phys. Fluids **34**, 073607 (2022); doi: 10.1063/5.0099475
Submitted: 17 May 2022 · Accepted: 24 June 2022 ·
Published Online: 14 July 2022

View Online Export Citation CrossMark

Ling Liu (刘玲),[1] Jing Li (李靖),[1,2,a),b)] and Shijun Liao (廖世俊)[1,2,c)]

AFFILIATIONS

[1]School of Naval Architecture, Ocean and Civil Engineering, Shanghai Jiao Tong University, Shanghai 200240, China
[2]State Key Laboratory of Ocean Engineering, Shanghai 200240, China

[a)]URL: https://lijing.sjtu.edu.cn/
[b)]Author to whom correspondence should be addressed: lijing_@sjtu.edu.cn
[c)]URL: https://sjliao.sjtu.edu.cn/

ABSTRACT

This paper describes explicit series solutions for supersonic flat-plate boundary layer flows that are convergent in the whole spatial domain for Mach numbers of up to 50. These series solutions are achieved by means of the homotopy analysis method (HAM), an analytic technique for highly nonlinear problems. Unlike the analytic approximations given by perturbation methods or other approaches, our explicit series solutions are guaranteed to converge with arbitrary physical parameters because of the so-called "convergence-control parameter" in the HAM framework. Explicit analytic expressions for the local surface skin-friction coefficient and the local heat-transfer coefficient of the supersonic boundary layer flow are also derived. These analytical solutions are found to be in perfect agreement with the corresponding numerical results, allowing the effects of physical parameters on supersonic boundary layer flows to be discussed in detail. The explicit series solutions described in this paper provide a benchmark for supersonic flat-plate boundary layer flows with Mach numbers in the range $0.8 \leq M_a \leq 50$. To the best of our knowledge, no such explicit series solutions for supersonic flat-plate boundary layer flows have previously been reported. To enable relevant applications, a corresponding Mathematica package is provided to enable convenient access to explicit series solutions for supersonic flat-plate boundary layer flows.

Published under an exclusive license by AIP Publishing. https://doi.org/10.1063/5.0099475

I. INTRODUCTION

Supersonic boundary layer flows are a major feature in high-speed aerodynamics, especially in the development of aviation and space technology. From flat plates to swept wings, and from subsonic to hypersonic Mach numbers, compressible boundary layer theory has been extensively studied and has greatly promoted the development of aerodynamics.[1–3] There has been widespread research on supersonic boundary layers. For example, the stability, sensitivity analysis, and receptivity of supersonic boundary layers have been studied by various numerical methods, such as the large-Reynolds-number approach,[4,5] Navier–Stokes approach,[6] and Muller's iteration techniques.[7] The experimental studies on the supersonic boundary layer have also been investigated by some researchers.[8,9] Yu and Luo[10] revealed the nonlinear interaction mechanisms of disturbances in supersonic flat-plate boundary layers through numerical simulations. Additionally, the supersonic flow around an infinitely thin plate perturbed by acoustic waves and the control of oblique breakdown in a supersonic boundary layer have been modeled using direct numerical simulation (DNS).[11,12] Recently, by combining the triple-deck theory and DNS, Liu *et al.*[13] investigated the excitation of the first Mack instability modes in a supersonic boundary layer due to the interaction between an acoustic wave and small streamwise isolated roughness elements on an otherwise flat plate. However, the above-mentioned studies are mostly based on numerical methods. To date, no explicit series solutions of supersonic boundary layer flows have been derived, mainly because the governing equations of supersonic boundary layers are coupled nonlinear differential equations and are thus very difficult to solve analytically. This provides the motivation for our study. This paper describes, for the first time, explicit series solutions of supersonic boundary layer flows that are valid in the whole spatial domain.

Even for the boundary layer flow of an incompressible fluid over a flat plate, there have been no reports of explicit series solutions that are valid in the whole domain. For instance, Blasius[14] derived a power series for the boundary layer equation of an incompressible fluid,

$$f(\eta) = \sum_{k=0}^{+\infty} \left(-\frac{1}{2}\right)^k \frac{A_k \sigma^{k+1}}{(3k+2)!} \eta^{3k+2}, \tag{1}$$

Published under an exclusive license by AIP Publishing

where A_k denotes the coefficients. Unfortunately, this is only convergent for small $\eta \leq 5.7$, meaning it is only valid in the flow field near the plate. To overcome this restriction, Blasius[14] established another asymptotic solution far from the plate and then matched this with the above power series solution near the plate.

Based on the concept of homotopy in topology, Liao[15–18] proposed an analytical method for highly nonlinear problems, namely, the homotopy analysis method (HAM). Unlike perturbation techniques,[19,20] the HAM framework does not depend on any small/large physical parameters. In particular, unlike all other techniques, the HAM guarantees the convergence of the series solution by means of an artificial convergence-control parameter. HAM has been widely applied in engineering,[21–25] finance,[26,27] biology,[28,29] quantum mechanics,[30,31] and other fields.[32,33] Note that Liao[34] used the HAM to derive, for the first time, an explicit series solution of Blasius' boundary layer flow that is valid in the whole flow field, $\eta \in [0, +\infty)$. Additionally, Xu *et al.*[35] first discovered the theoretical existence of steady-state exactly resonant gravity waves (with a time-independent wave spectrum) in water of a finite depth by means of the HAM, and Liu *et al.*[36] combined the HAM with the Galerkin method to obtain finite-amplitude steady-state resonant wave groups in finite water depths. Recently, Xu and Liu[37] obtained nonlinear steady-state resonant waves in water of finite depth using an amplitude-based HAM. Furthermore, Liao *et al.*[38] successfully used the HAM to obtain steady-state nearly resonant waves, and Yang *et al.*[39] discovered the existence of steady-state resonant acoustic-gravity waves through the application of the HAM, indicating the widespread existence of steady-state resonant waves. The HAM was used by Zhong and Liao[40] to obtain, for the first time, the convergent series solution of the limiting Stokes wave of maximum amplitude for *arbitrary* water depths. Massa and Schetz[41] extended the HAM to the multidimensional reconstruction of heat flux and validated the output using hypersonic wind tunnel tests. More importantly, Jiang *et al.*[42] derived the sensitivity of boundary layer stability to certain flow parameters analytically using the HAM. All of these successful applications demonstrate the great potential and superiority of the HAM, encouraging us to apply this framework to the supersonic boundary layer problem considered in this paper.

II. MATHEMATICAL FORMULATION

A. Governing equations

Consider a two-dimensional, steady, compressible flow over a flat plate with constant wall conditions. According to Refs. 43 and 44, the compressible boundary layer equations read

$$Cf'''(\eta) + f(\eta)f''(\eta) = 0, \tag{2}$$

$$Cg''(\eta) + P_r f(\eta)g'(\eta) + (\gamma - 1)M_a^2 P_r Cf''2(\eta) = 0, \tag{3}$$

with boundary conditions

$$f(0) = 0,\ f'(0) = 0,\ f'(+\infty) = 1,\ g(0) = T_w^*,\ g(+\infty) = 1, \tag{4}$$

where the primes denote differentiation with respect to η, M_a is the Mach number, $f'(\eta) = u/u_e$, $g = g(\eta) = h/h_e$, $Pr = \mu c_p/k$ is the Prandtl number, and $C = \rho\mu/(\rho_e\mu_e)$. Here, the velocity u, density ρ, and fluid enthalpy h are unknown physical quantities, and the viscosity coefficient μ and thermal conductivity k are temperature-dependent properties of the fluid. u_e, h_e, ρ_e, and μ_e denote the velocity, enthalpy, density, and viscosity coefficients of the free-stream at the edge of the supersonic boundary layer, respectively. We assume that the oncoming fluid is gas and C is a constant. Let us consider the standard Prandtl number $P_r = 0.72$ and the specific heat ratio $\gamma = 1.4$ for air. The dimensionless constant wall temperature T_w^* is defined as[13,45]

$$T_w^* = \frac{T_w}{T_e} = 1 + \sqrt{P_r}(\gamma - 1)M_a^2/2, \tag{5}$$

where T_w and T_e represent the dimensional constant wall temperature and free-stream temperature, respectively.

According to the above description, the displacement thickness δ^* can be written as

$$\delta^* = \sqrt{2}L^* R^{-\frac{1}{2}} \int_0^{+\infty} \left[g(\eta) - f'(\eta)\right] d\eta, \tag{6}$$

where L^* is a distance downstream of the leading edge and R is the Reynolds number based on the distance to the leading edge.

The physical parameters of interest are the local surface skin-friction coefficient c_f, which is related to the velocity at the wall given by $f''(0)$, and the local heat-transfer rate at the surface, which is related to the enthalpy gradient $g'(0)$. We express c_f as

$$c_f = \frac{\tau_w}{\frac{1}{2}\rho_e u_e^2} = \frac{2}{\rho_e u_e^2}\left[\mu\left(\frac{\partial u}{\partial y}\right)\right]_w = \frac{\sqrt{2}C_w f''(0)}{\sqrt{Re_x}}, \tag{7}$$

where $Re_x = \rho_e u_e x/\mu_e$ is the local Reynolds number and C_w is a physical parameter representing the variation of viscosity with temperature. This can be defined using Sutherland's law as

$$C_w = \frac{\mu_w^*}{T_w^*} = \left(\frac{T_w}{T_e}\right)^{1/2} \frac{T_e + S}{T_w + S}, \tag{8}$$

where μ_w^* is the dimensionless viscosity coefficient at the wall, $S = 110$ K is Sutherland's constant for air, and $T_w = T_w^* T_e$.

The local heat-transfer coefficient can be expressed by the Stanton number C_H defined as

$$C_H = \frac{c_f}{2Pr^{2/3}}, \tag{9}$$

which is a form of the Reynolds analogy.

The coupled nonlinear system of differential equations given by (2) and (3) might not seem complicated, but it is difficult to solve analytically. This paper is devoted to obtaining explicit, analytic approximate solutions and studying the principal effects of a high Mach number, skin-friction, and heat transfer by solving Eqs. (2)–(4) using HAM.

B. HAM approach

In this section, HAM is used to derive an explicit series solution of the supersonic boundary-layer equations stated above. For simplicity, let us take the transformation

$$\xi = \lambda\eta, \quad F(\xi) = f(\eta), \quad S(\xi) = g(\eta), \tag{10}$$

where $\lambda > 0$ is the spatial scale factor. Note that the purpose of this transformation is to separate the spatial scale factor λ from the exponent of the solution expression (15) and (16) in order to improve the

Published under an exclusive license by AIP Publishing

computational efficiency. Moreover, λ is introduced to help us adjust the exponential scale and obtain the convergent series solutions. Then, Eqs. (2) and (3) become

$$C\lambda F'''(\xi) + F(\xi)F''(\xi) = 0, \tag{11}$$

$$C\lambda S''(\xi) + P_r F(\xi)S'(\xi) + (\gamma - 1)M_a^2 P_r C\lambda^3 F''^2(\xi) = 0, \tag{12}$$

with the boundary conditions

$$F(0) = 0, \quad F'(0) = 0, \quad F'(+\infty) = \frac{1}{\lambda}, \quad S(0) = T_w^*, \quad S(+\infty) = 1. \tag{13}$$

According to the boundary conditions in Eq. (4), both $f'(\eta)$ and $g(\eta)$ approach 1 as $\eta \to +\infty$, indicating that $F(\xi)$ and $S(\xi)$ should decay exponentially at infinity. Thus, we choose a set of base functions

$$\{1, \xi, \xi^n \exp(-m\xi) \mid n \geq 0, m \geq 1\}, \tag{14}$$

for $F(\xi)$ and $S(\xi)$, e.g.,

$$F(\xi) = \xi + \sum_{m=1}^{+\infty} \sum_{n=0}^{+\infty} a_{m,n}\, \xi^n \exp(-m\xi), \tag{15}$$

$$S(\xi) = 1 + \sum_{m=1}^{+\infty} \sum_{n=0}^{+\infty} b_{m,n}\, \xi^n \exp(-m\xi), \tag{16}$$

where $a_{m,n}$ and $b_{m,n}$ are constant coefficients to be determined by HAM.

According to the solution expressions in Eqs. (15) and (16) and using the boundary conditions in Eq. (13), the initial guess is

$$F_0(\xi) = \frac{\xi}{\lambda} - \frac{1}{\lambda} + \frac{1}{\lambda} e^{-\xi}, \tag{17}$$

$$S_0(\xi) = 1 + (T_W^* - 1)e^{-\xi}. \tag{18}$$

According to the solution expressions of Eqs. (15) and (16), we choose the auxiliary linear operators

$$\mathscr{L}_F[\Phi(\xi;q)] = \frac{d^3\Phi}{d\xi^3} + \frac{d^2\Phi}{d\xi^2}, \tag{19}$$

$$\mathscr{L}_S[\Theta(\xi;q)] = \frac{d^2\Theta}{d\xi^2} + \frac{d\Theta}{d\xi}, \tag{20}$$

with the properties

$$\mathscr{L}_F[C_1\xi + C_2 \exp(-\xi) + C_3] = 0, \tag{21}$$

$$\mathscr{L}_S[C_4 + C_5 \exp(-\xi)] = 0, \tag{22}$$

where C_1, C_2, C_3, C_4, and C_5 are constants. According to Eqs. (11) and (12), we define the following nonlinear operators:

$$\mathscr{N}_F[\Phi(\xi;q)] = C\lambda \frac{\partial^3\Phi(\xi;q)}{\partial\xi^3} + \Phi(\xi;q)\frac{\partial^2\Phi(\xi;q)}{\partial\xi^2}, \tag{23}$$

$$\mathscr{N}_S[\Phi(\xi;q), \Theta(\xi;q)] = C\lambda \frac{\partial^2\Theta(\xi;q)}{\partial\xi^2} + P_r\Phi(\xi;q)\frac{\partial\Theta(\xi;q)}{\partial\xi} + (\gamma - 1)M_a^2 P_r C\lambda^3 \left[\frac{\partial^2\Phi(\xi;q)}{\partial\xi^2}\right]^2, \tag{24}$$

where $q \in [0,1]$ is an embedding parameter and $\Phi(\xi;q)$, $\Theta(\xi;q)$ are functions of ξ and q. Let $c_0 \neq 0$ denote the convergence-control parameter. We construct the so-called zeroth-order deformation equations

$$(1-q)\mathscr{L}_F[\Phi(\xi;q) - F_0(\xi)] = q\, c_0 \mathscr{N}_F[\Phi(\xi;q)], \tag{25}$$

$$(1-q)\mathscr{L}_S[\Theta(\xi;q) - S_0(\xi)] = q\, c_0 \mathscr{N}_S[\Phi(\xi;q), \Theta(\xi;q)], \tag{26}$$

subject to the boundary conditions

$$\Phi(0;q) = 0, \quad \Phi'(0;q) = 0, \quad \Phi'(+\infty;q) = \frac{1}{\lambda}, \quad \Theta(0;q) = T_w^*, \quad \Theta(+\infty;q) = 1, \tag{27}$$

where $q \in [0,1]$ is an embedding parameter.

Because the initial guesses $F_0(\xi)$ and $S_0(\xi)$ satisfy the boundary conditions (13), and from definitions (25) and (26), we have the following at $q = 0$:

$$\Phi(\xi;0) = F_0(\xi), \quad \Theta(\xi;0) = S_0(\xi). \tag{28}$$

At $q = 1$, the zeroth-order deformation equations (25)–(27) are exactly the same as the original equations (11)–(13), respectively, so that we have

$$\Phi(\xi;1) = F(\xi), \quad \Theta(\xi;1) = S(\xi). \tag{29}$$

Therefore, as q increases from 0 to 1, $\Phi(\xi;q)$ and $\Theta(\xi;q)$ vary (or deform) continuously from the initial guesses $F_0(\xi)$ and $S_0(\xi)$ to the solutions $F(\xi)$ and $S(\xi)$ of Eqs. (11)–(13), respectively. This is why Eqs. (25)–(27) are called the zeroth-order deformation equations.

Using the Taylor's expansions of $\Phi(\xi;q)$ and $\Theta(\xi;q)$ about q at $q = 0$, we then obtain

$$\Phi(\xi;q) = F_0(\xi) + \sum_{n=1}^{+\infty} F_n(\xi) q^n, \tag{30}$$

$$\Theta(\xi;q) = S_0(\xi) + \sum_{n=1}^{+\infty} S_n(\xi) q^n, \tag{31}$$

where

$$F_n(\xi) = \frac{1}{n!}\frac{\partial^n\Phi(\xi;q)}{\partial q^n}\bigg|_{q=0}, \quad S_n(\xi) = \frac{1}{n!}\frac{\partial^n\Theta(\xi;q)}{\partial q^n}\bigg|_{q=0}. \tag{32}$$

Here, it should be emphasized that, different from other techniques such as perturbation methods, HAM uses the convergence-control parameter c_0, whose value can be freely determined. Assuming that the convergence-control parameter c_0 is chosen such that the above Taylor expansions converge at $q = 1$, Eq. (29) leads to the so-called homotopy-series solutions,

$$F(\xi) = \Phi(\xi;1) = F_0(\xi) + \sum_{n=1}^{+\infty} F_n(\xi), \tag{33}$$

$$S(\xi) = \Theta(\xi;1) = S_0(\xi) + \sum_{n=1}^{+\infty} S_n(\xi). \tag{34}$$

Thus, the corresponding Mth-order approximations are

$$F(\xi) \approx F_0(\xi) + \sum_{n=1}^{M} F_n(\xi), \tag{35}$$

$$S(\xi) \approx S_0(\xi) + \sum_{n=1}^{M} S_n(\xi), \tag{36}$$

Published under an exclusive license by AIP Publishing

where $F_n(\xi)$ and $S_n(\xi)$ are governed by the so-called nth-order deformation equations,

$$\mathscr{L}_F[F_n(\xi) - \chi_n F_{n-1}(\xi)] = c_0\,\delta^F_{n-1}(\xi), \tag{37}$$

$$\mathscr{L}_S[S_n(\xi) - \chi_n S_{n-1}(\xi)] = c_0\,\delta^S_{n-1}(\xi), \tag{38}$$

subject to the boundary conditions

$$F_n(0) = F_n'(0) = F_n'(+\infty) = 0, \quad S_n(0) = S_n(+\infty) = 0, \tag{39}$$

where

$$\chi_n = \begin{cases} 0, & \text{when } n \le 1, \\ 1, & \text{otherwise} \end{cases} \tag{40}$$

and

$$\delta^F_k(\xi) = C\lambda F_k'''(\xi) + \sum_{i=0}^{k} F_i''(\xi) F_{k-i}(\xi), \tag{41}$$

$$\delta^S_k(\xi) = C\lambda S_k''(\xi) + Pr\sum_{i=0}^{k} F_{k-i}(\xi) S_i'(\xi) + (\gamma-1) M_a^2 Pr\, C\lambda^3 \sum_{i=0}^{k} F_i''(\xi) F_{k-i}''(\xi), \tag{42}$$

are obtained by substituting Eqs. (30) and (31) into the zeroth-order deformation equations (25)–(27) and evaluating like-powers of q.

A key question is whether the series solutions (33) and (34) convergent in the whole domain $\eta \in [0, +\infty)$. Fortunately, unlike other techniques such as perturbation methods, HAM guarantees the convergence of series solutions through the convergence-control parameter c_0. Note that, in the HAM framework, c_0 has *no* physical meaning, and we have *significant* freedom to choose its value. There often exists an interval $\mathscr{R}$ such that each $c_0 \in \mathscr{R}$ gives the *same* convergent series solution with different convergence rates. The optimal value of c_0 is determined by minimizing the square of the total residual error $\varepsilon_M^{total}(c_0)$ at the Mth-order approximation, i.e.,

$$\varepsilon_M^{total}(c_0) = \varepsilon_M^F(c_0) + \varepsilon_M^S(c_0),$$

where

$$\varepsilon_M^F(c_0) = \frac{1}{N+1}\sum_{j=0}^{N}\left[\mathscr{N}_F\left(\sum_{i=0}^{M} F_i(\xi)\right)\Big|_{\xi=j\delta\xi}\right]^2, \tag{43}$$

$$\varepsilon_M^S(c_0) = \frac{1}{N+1}\sum_{j=0}^{N}\left[\mathscr{N}_S\left(\sum_{i=0}^{M} F_i(\xi), \sum_{i=0}^{M} S_i(\xi)\right)\Big|_{\xi=j\delta\xi}\right]^2, \tag{44}$$

in which M is the order of approximation, N is a sufficiently large integer, and $\varepsilon_M^F(c_0)$, $\varepsilon_M^S(c_0)$ denote the squares of the residual errors from the two equations governing the supersonic boundary layer flow. When M is large enough, c_0 has nothing to do with the order of approximation.

C. Explicit series solutions for $f(\eta)$ and $g(\eta)$

It is not difficult to solve the linear high-order deformation equations (37)–(39) individually, especially by means of the Mathematica software. Following Liao, this gives the explicit series solution of the supersonic boundary layer problem, i.e., $f(\eta)$ and $g(\eta)$ governed by Eqs. (2) and (3).

First, we find the general expressions of F_m and S_m for arbitrary $m \ge 0$, which contain many unknown coefficients. The recurrence formulas of these coefficients are then derived manually using the high-order deformation equations (37)–(39) and the initial guesses. Finally, we gain the series solutions of $f(\eta)$ and $g(\eta)$,

$$f(\eta) = \eta + \lim_{M\to+\infty}\sum_{m=0}^{M} b^0_{m,0} + \lim_{M\to+\infty}\sum_{n=1}^{M+1}\exp(-n\lambda\eta) \times \left(\sum_{m=n-1}^{M}\sum_{k=0}^{2(m+1-n)} b^k_{m,n}(\lambda\eta)^k\right) \tag{45}$$

and

$$g(\eta) = 1 + \lim_{M\to+\infty}\sum_{n=1}^{M+1}\exp(-n\lambda\eta) \times \left(\sum_{m=n-1}^{M}\sum_{l=0}^{2(m+1-n)} d^l_{m,n}(\lambda\eta)^l\right), \tag{46}$$

where $b^k_{m,n}$ and $d^l_{m,n}$ are the constant coefficients of $f(\eta)$ and $g(\eta)$ (see Appendixes A and B, respectively).

Note that the coefficients $b^k_{m,n}$ and $d^l_{m,n}$ can be obtained in order by means of the recurrence formulas listed in Appendixes A and B. In this way, we obtain the Mth-order approximation of the supersonic boundary layer flow. For a detailed derivation, please refer to the process applied by Liao.[34]

D. Choice of the convergence-control parameter c_0

The explicit series solutions for $f(\eta)$ and $g(\eta)$ in Eqs. (45) and (46) contain the physical parameters C and M_a as well as the spatial scale factor λ and the convergence-control parameter c_0. The values of λ and c_0 are allowed to be selected manually. Following Liao,[34] we simply choose $\lambda = 4$. Then, $\forall M_a \in [0.8, 50]$, we can obtain convergent series solutions by means of the following empirical formula for the convergence-control parameter:

$$c_0 = -1.23e^{-3.238C} - 0.3761e^{-0.5518C}, \quad 0.5 \le C \le 1.5. \tag{47}$$

We emphasize that neither the original governing equations (2)–(4) nor our HAM method have any restriction on Mach number. The choice of this interval of the Mach number is mainly from the practical aspects. In the present study, we give a unified spatial scale factor $\lambda = 4$ and obtain the empirical formula (47), which is valid not only for supersonic boundary layer flows ($1 \le M_a \le 5$), but also for high subsonic ($0.8 \le M_a \le 1$) and hypersonic boundary layer flows with Mach numbers M_a of up to 50. This large range of the Mach number provides us the confidence to cover most industrial use. However, there is no limit for the HAM to solve this equation no matter what the Mach number is. Even for Mach numbers higher than 50, the HAM may not easy to converge by using the current parameters, but the convergence can always be guaranteed by adjusting the values of the spatial scale factor and convergence-control parameters.

Published under an exclusive license by AIP Publishing

The freedom to choose these parameters to ensure the convergence is the significant icon of the HAM. Besides, according to Sutherland's law, the range of C in this formula covers the incoming air temperatures commonly used in wind tunnel experiments. Therefore, the empirical formula (47) is useful in practice.

The value of $c_0 = -1$ corresponds to an approximation given by some other methods, such as the famous "Lyapunov artificial small parameter method." However, the series solutions in Eqs. (45) and (46) are divergent when $c_0 = -1$. This indicates the importance of the convergence-control parameter c_0 in the HAM framework and illustrates the great potential of HAM. In fact, it is the convergence-control parameter that differentiates HAM from all other approximation techniques.

E. Explicit formulas for c_f and C_H

In theory, the explicit series solutions of Eqs. (45) and (46) lead to the local surface skin-friction coefficient c_f and the local heat-transfer coefficient C_H. For simplicity, we present the following tenth-order approximation of c_f:

$$c_f\sqrt{Re_x} = C_w \sum_{k=0}^{10} \alpha_k C^k, \tag{48}$$

where C_w is defined by Eq. (8) and α_k is a coefficient that depends on the convergence-control parameter c_0,

$$\begin{aligned}\alpha_0 &= 4 - 5c_0 - 9.375c_0^2 - 28.646c_0^3 - 88.94c_0^4 \\ &\quad - 249.811c_0^5 - 597.529c_0^6 - 1153.653c_0^7 \\ &\quad - 1676.63c_0^8 - 1626.916c_0^9 - 789.930c_0^{10}, \end{aligned}\tag{49}$$

$$\begin{aligned}\alpha_1 &= 160c_0 + 100c_0^3 + 401.042c_0^4 + 1280.738c_0^5 \\ &\quad + 3330.82c_0^6 + 6828.906c_0^7 + 10382.876c_0^8 \\ &\quad + 10432.362c_0^9 + 5206.132c_0^{10}, \end{aligned}\tag{50}$$

$$\begin{aligned}\alpha_2 &= 2880c_0^2 - 962.5c_0^5 - 4269.125c_0^6 \\ &\quad - 11419.954c_0^7 - 20486.719c_0^8 \\ &\quad - 23073.057c_0^9 - 12518.834c_0^{10}, \end{aligned}\tag{51}$$

$$\begin{aligned}\alpha_3 &= 30720c_0^3 + 3252.667c_0^7 + 11419.954c_0^8 \\ &\quad + 18210.417c_0^9 + 12305.613c_0^{10}, \end{aligned}\tag{52}$$

$$\alpha_4 = 215040c_0^4 - 2537.768c_0^9 - 3642.083c_0^{10}, \tag{53}$$

$$\alpha_5 = 1.032 \times 10^6 c_0^5, \tag{54}$$

$$\alpha_6 = 3.441 \times 10^6 c_0^6, \tag{55}$$

$$\alpha_7 = 7.864 \times 10^6 c_0^7, \tag{56}$$

$$\alpha_8 = 1.180 \times 10^7 c_0^8, \tag{57}$$

$$\alpha_9 = 1.049 \times 10^7 c_0^9, \tag{58}$$

$$\alpha_{10} = 4.194 \times 10^6 c_0^{10}, \tag{59}$$

in which we use the optimal c_0 defined by Eq. (47). Then, we can further obtain C_H from Eq. (9).

Note that, with the optimal convergence-control parameter of Eq. (47), the tenth-order approximations of c_f and C_H are sufficiently accurate, as shown in Fig. 1, where the tenth-order approximation from Eq. (48) is in good agreement with the 25th-order approximation of c_f. This again illustrates the importance of c_0 in elevating HAM above other approximation methods.

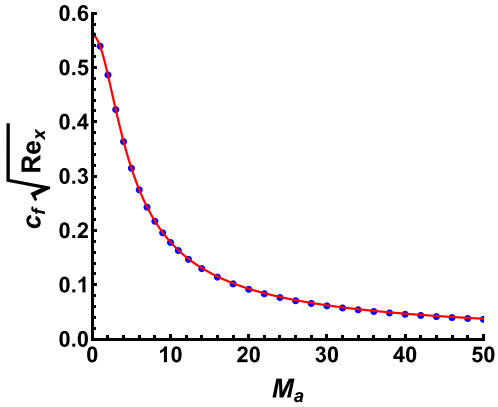

FIG. 1. Comparison of the tenth-order approximation (48) of c_f with the 25th-order convergent solution of c_f for $C = 1.4$. Solid line: tenth-order approximation (48); circles: 25th-order convergent solution of c_f.

III. RESULTS AND ANALYSIS

Without loss of generality, let us first consider the case $C = 1$, $M_a = 4$ so as to verify the validity of the series solutions given by Eqs. (45) and (46). Using $c_0 = -0.2649$ from Eq. (47) and $\lambda = 4$, we indeed gain the convergent solution $f''(0) = 0.469\,59$, as shown in Table I. This agrees well with the homotopy-Padé approximation, obtained using a technique combining Padé approximation and HAM.[18] Furthermore, our convergent series solutions $f'(\eta)$ and $g'(\eta)$ agree well with the corresponding numerical results given by the finite difference method with the three-stage Lobatto IIIa formula,[46] as shown in Fig. 2. Comparing the series solution with the numerical results for $C = 0.6$ and $C = 1.5$ when $M_a = 4$, we find that our series solutions match the numerical ones quite well, as shown in Figs. 3 and 4. We further investigate the convergent series solutions of $f'(\eta)$ and $g(\eta)$ at $M_a = 0.8$ and $M_a = 50$ for the case of $C = 1$. Table II quantitatively shows the comparison between the convergent series solutions of $f'(\eta)$ and $g(\eta)$ and numerical results. For smaller values of M_a, our HAM solutions match the numerical results exactly. Even if the value of M_a is as high as 50, our convergent series solutions still have a precision of $1 - 3$ decimal places compared with the numerical results. The matching curves of the convergent series solutions and numerical

TABLE I. Homotopy approximations and $[m, m]$ homotopy-Padé approximations of $f''(0)$ for $C = 1$, $M_a = 4$ given by $\lambda = 4$ and $c_0 = -0.2649$.

m, order of approx.	$f''(0)$	m	$f''(0)$ given by the $[m, m]$ homotopy-Padé approx.
5	0.441 52	5	0.469 12
8	0.467 97	7	0.469 54
9	0.468 27	8	0.469 59
15	0.469 48	9	0.469 59
20	0.469 58	10	0.469 59
22	0.469 59	11	0.469 59
24	0.469 59	12	0.469 59

Published under an exclusive license by AIP Publishing

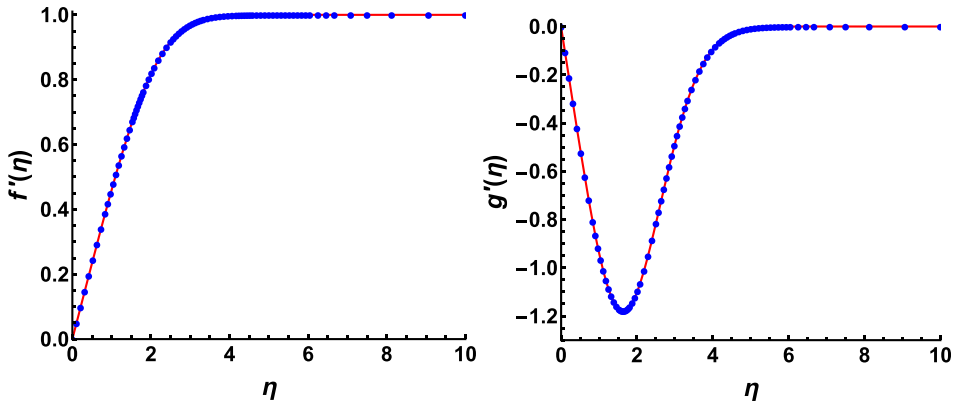

FIG. 2. Comparison of the convergent homotopy approximation $f'(\eta)$ and $g'(\eta)$ with the numerical result for $C = 1$ and $M_a = 4$. Solid line: convergent homotopy approximation given by $c_0 = -0.2649$ and $\lambda = 4$; symbols: numerical results. (a) $f'(\eta)$; and (b) $g'(\eta)$.

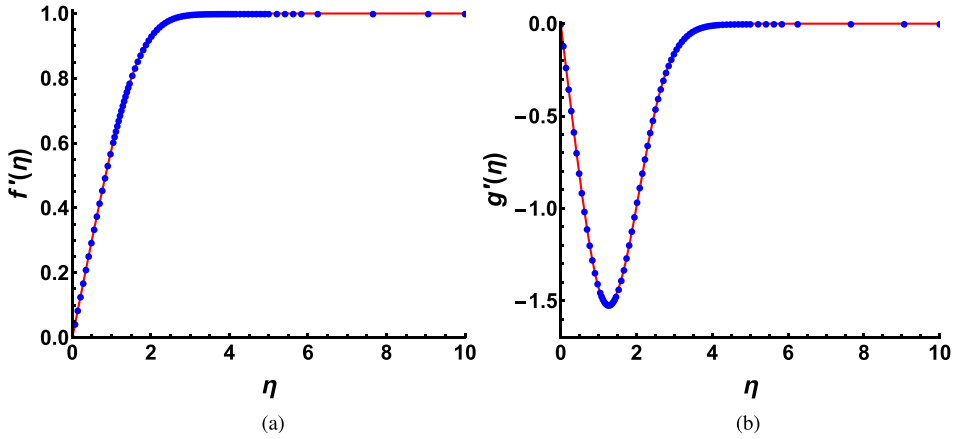

FIG. 3. Comparison of the convergent homotopy approximations $f'(\eta)$ and $g'(\eta)$ with the numerical results for $C = 0.6$ and $M_a = 4$. Solid line: convergent homotopy approximation given by $c_0 = -0.4464$ and $\lambda = 4$; symbols: numerical results. (a) $f'(\eta)$; and (b) $g'(\eta)$.

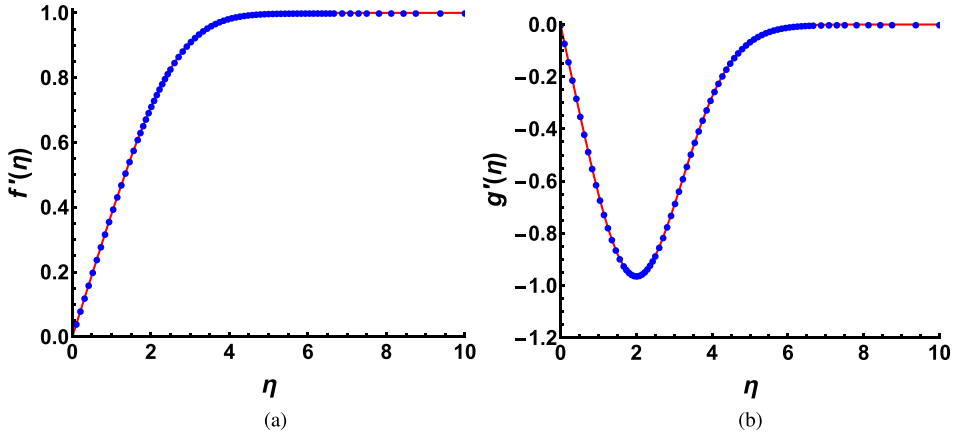

FIG. 4. Comparison of the convergent homotopy approximations $f'(\eta)$ and $g'(\eta)$ with the numerical results for $C = 1.5$ and $M_a = 4$. Solid line: convergent homotopy approximation given by $c_0 = -0.1740$ and $\lambda = 4$; symbols: numerical results. (a) $f'(\eta)$; and (b) $g'(\eta)$.

results of $g(\eta)$ at $M_a = 0.8,\ 50$ are clearly shown in Fig. 5. All of these results indicate the validity of our series solutions in Eqs. (45) and (46) for supersonic boundary layer flows.

Next, we investigate the influence of C and M_a in Eqs. (45) and (46). First, the influence of C on the velocity profile $f'(\eta)$ and the temperature distribution $g(\eta)$ is shown in Fig. 6. In Fig. 6(a), $f'(\eta)$ exhibits a decreasing trend as C increases, and the greater velocity of the internal flow corresponds to a thinner boundary layer. The growth of C leads to an increase in temperature at the same height level of the boundary layer [see Fig. 6(b)]. Recall that an increase in C indicates a stronger coupling degree of the governing equations.

Figure 7 presents the influence of M_a on the temperature profile $g(\eta)$ and its rate of change $g'(\eta)$. From Fig. 7(a), we find that the convergent $g'(\eta)$ decreases as M_a increases from 2 to 5. In other words,

Published under an exclusive license by AIP Publishing

TABLE II. Comparison of convergent series solutions (HAM) of $f'(\eta)$ and $g(\eta)$ with the numerical results (Num) at $M_a = 0.8$ and $M_a = 50$ in the case of $C = 1$.

	$M = 0.8$				$M = 50$			
	$f'(\eta)$		$g(\eta)$		$f'(\eta)$		$g(\eta)$	
parameters η	HAM	Num	HAM	Num	HAM	Num	HAM	Num
0.000	0.000	0.000	1.109	1.109	0.000	0.000	425.264	425.264
0.139	0.065	0.065	1.108	1.108	0.065	0.065	423.712	423.709
0.417	0.195	0.195	1.105	1.105	0.195	0.195	411.444	411.443
0.833	0.387	0.387	1.095	1.095	0.387	0.387	371.013	371.013
1.111	0.508	0.508	1.085	1.085	0.508	0.508	331.268	331.267
1.458	0.646	0.646	1.069	1.069	0.646	0.646	271.721	271.746
2.014	0.820	0.820	1.044	1.044	0.820	0.820	171.226	171.209
2.569	0.927	0.927	1.023	1.023	0.927	0.927	89.289	89.126
3.056	0.973	0.973	1.011	1.011	0.973	0.973	43.106	43.082
3.542	0.992	0.992	1.004	1.004	0.992	0.992	18.151	18.259
4.097	0.998	0.998	1.001	1.001	0.998	0.998	6.046	6.168
4.931	1.000	1.000	1.000	1.000	1.000	1.000	1.537	1.579
5.833	1.000	1.000	1.000	1.000	1.000	1.000	1.027	1.032
6.806	1.000	1.000	1.000	1.000	1.000	1.000	1.006	1.001
7.917	1.000	1.000	1.000	1.000	1.000	1.000	1.000	1.000
9.375	1.000	1.000	1.000	1.000	1.000	1.000	1.000	1.000
10.000	1.000	1.000	1.000	1.000	1.000	1.000	1.000	1.000

the temperature change becomes faster as the Mach number increases. This implies that more heat can be distributed, because a larger M_a leads to an increment in the wall temperature [see Fig. 7(b)]. We also investigate the impact of C and M_a on the displacement thickness δ^*. As shown in Fig. 8, the displacement thickness given by Eq. (6) is proportional to C and M_a. In fact, in hypersonic flows, this phenomenon becomes more pronounced.

The characteristic properties of the skin friction coefficient c_f and heat transfer coefficient C_H with respect to M_a are now discussed. As noted in Sec. II E, the tenth-order approximations of c_f [Eq. (48)] and C_H can be calculated and analyzed $\forall C \in [0.5, 1.5]$. We restrict our interest to $C = 0.5$, 0.9, 1.2, and 1.5 for the comparisons of c_f and C_H. For clarity, Fig. 9(a) shows that c_f gradually decreases as C changes from 0.5 to 1.5. This is reasonable—in fact, the velocity gradient $(\frac{\partial u}{\partial y})_w$ decreases as C increases [see Fig. 6(a)]. Thus, the tangential stress $\tau_w = \mu(\frac{\partial u}{\partial y})_w$ and $c_f = 2\tau_w/\rho_e u_e^2$ naturally decrease. Additionally, we can see that c_f decreases as the Mach number increases from 0 to 50. However, this does not mean that the tangential stress τ_w on the plate exhibits the same trend, despite a gradual decline in c_f.

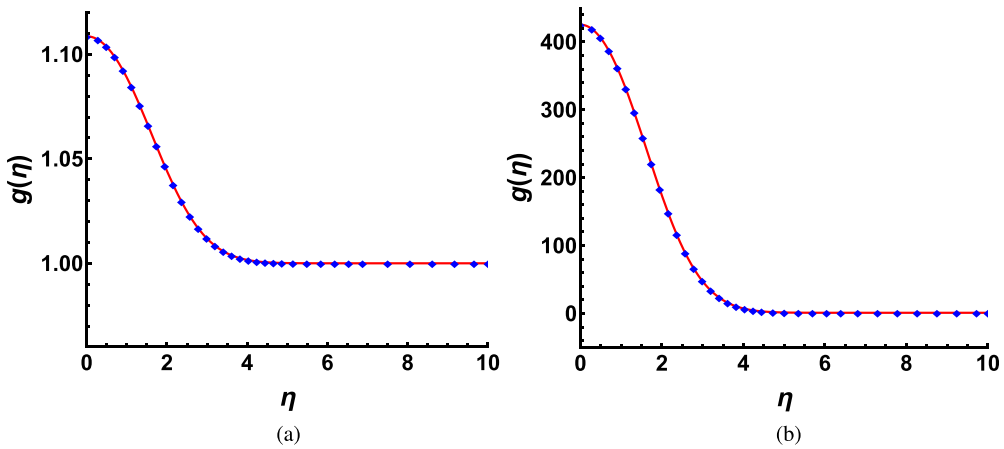

FIG. 5. Comparison of the convergent homotopy approximations $g(\eta)$ with the numerical results in the case of $C = 1$. Solid line: convergent homotopy approximation given by $c_0 = -0.2649$ and $\lambda = 4$; symbols: numerical results. (a) $g(\eta)$ at $M_a = 0.8$; and (b) $g(\eta)$ at $M_a = 50$.

Published under an exclusive license by AIP Publishing

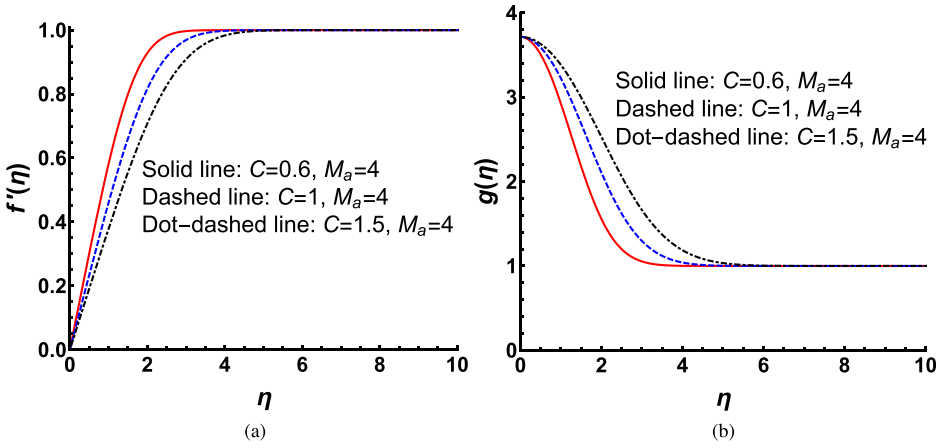

FIG. 6. Velocity profile $f'(\eta)$ and temperature profile distribution $g(\eta)$ with different values of C for $M_a = 4$. Solid line: $C = 0.6$; dashed line: $C = 1$; dot-dashed line: $C = 1.5$. (a) $f'(\eta)$; and (b) $g(\eta)$.

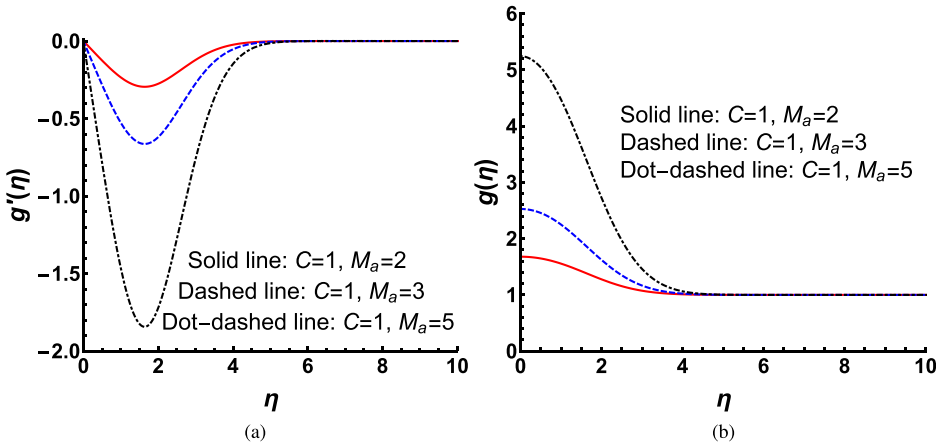

FIG. 7. Rate of temperature $g'(\eta)$ and temperature profile distributions $g(\eta)$ with different values of Mach number M_a for $C = 1$. Solid line: $M_a = 2$; dashed line: $M_a = 3$; dot-dashed line: $M_a = 5$. (a) $g'(\eta)$; and (b) $g(\eta)$.

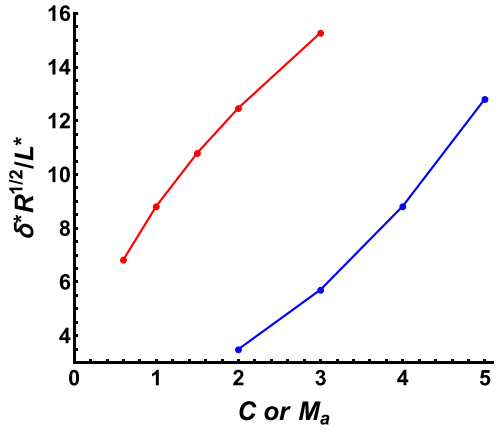

FIG. 8. Displacement thickness of boundary layer with respect to C or Mach number M_a. Red markers: δ^* with respect to C; blue markers: δ^* with respect to Mach number M_a.

Because $\tau_w = \frac{1}{2}\rho_e u_e^2 c_f = \frac{1}{2}\gamma\rho_e RT\frac{u_e^2}{a_e^2}c_f = \frac{1}{2}\gamma p_e M_a^2 c_f$, we find that τ_w increases as a result of the M_a^2 term.

Finally, the predicted heat transfer [see Fig. 9(b)] exhibits a similar trend to the skin friction with respect to the Mach number thanks to the Reynolds analogy of Eq. (9).

IV. CONCLUDING REMARKS

In this study, the supersonic boundary layer flow has been analytically solved using HAM, a powerful tool for highly nonlinear problems. The explicit series solutions of $f(\eta)$ and $g(\eta)$, governed by Eqs. (45) and (46), have been derived for the first time. Note that these explicit series solutions are valid in the *whole* region $\eta = [0, +\infty)$ and are therefore different from the approximations given by *all* other methods. The recurrence formulas for the constant coefficients, i.e., Eqs. (A1)–(A9) and (B1)–(B8), have been presented in detail, and the corresponding Mathematica code is available online for the convenience of its application. Different from perturbation methods and other techniques, the empirical formula in Eq. (47) gives the so-called

Published under an exclusive license by AIP Publishing

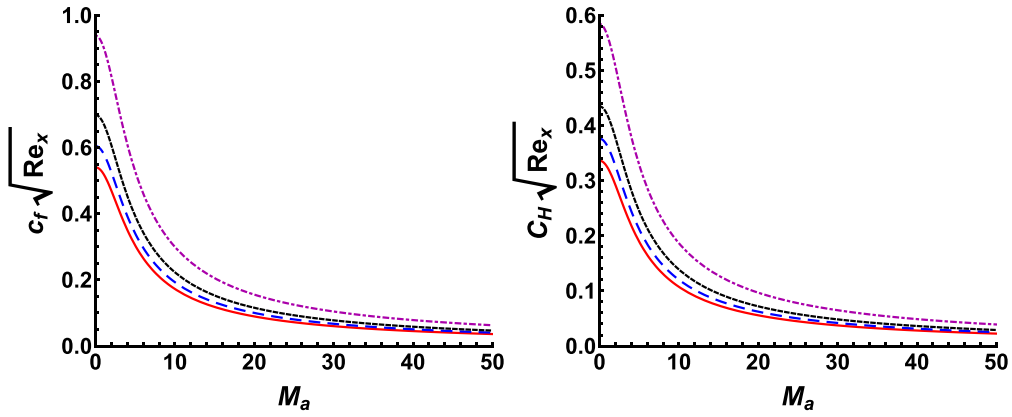

FIG. 9. Flat-plate skin friction c_f and heat transfer C_H with respect to Mach number, $T_e = 288$ K. Dot-dashed line (magenta): $C = 0.5$; short-dashed line (black): $C = 0.9$; long-dashed line (blue): $C = 1.2$; solid line (red): $C = 1.5$. (a) c_f with various M_a; and (b) C_H with various M_a.

convergence-control parameter c_0 in the HAM framework, which guarantees the convergence of the explicit series solutions. In addition, explicit series formulas for the local surface skin-friction coefficient c_f and the local heat-transfer coefficient C_H of the supersonic boundary layer flow have been derived for the first time. These are valid for Mach numbers in the range $0.8 \le M_a \le 50$. All of these explicit series solutions provide benchmarks for supersonic boundary layer flows.

To validate our explicit series solutions, we conducted a thorough comparison with numerical solutions. The velocity profile and temperature distribution under $C = 0.6$, 1, and 1.5 were investigated, and perfect agreement with numerical results was obtained. The analytical and numerical solutions still match well when the Mach number reaches 50, which verifies the accuracy of our explicit series solutions. This approach can be used to study more complicated supersonic/hypersonic boundary layer problems including stability analysis or shock wave problems, as will be considered in future work.

For the sake of application, we have developed a *Mathematica* package[47] for the explicit series solutions derived in this study, which is available online (see the supplementary material). Users need only input the values of the two physical parameters C and M_a in the supersonic/hypersonic boundary layer problem, and the convergent solution is given quickly by the program package.

SUPPLEMENTARY MATERIAL

See the supplementary material for a Mathematica code for the series solution https://lijing.sjtu.edu.cn/codes/liuling2022pof.zip.

ACKNOWLEDGMENTS

This work is partly supported by the National Natural Science Foundation of China (Grant No. 91752104). Partially supported by Shanghai Pilot Program for Basic Research - Shanghai Jiao Tong University (No. 21TQ1400202).

AUTHOR DECLARATIONS

Conflict of Interest

The authors have no conflicts to disclose.

Author Contributions

Ling Liu: Formal analysis (lead); Investigation (lead); Methodology (lead); Software (lead); Writing – original draft (lead). **Jing Li:** Supervision (equal); Validation (equal); Writing – review and editing (equal). **S. Liao:** Funding acquisition (lead); Supervision (equal); Writing – review and editing (equal).

DATA AVAILABILITY

The data that support the findings of this study are available within the article and its supplementary material.

APPENDIX A: COEFFICIENTS OF THE EXPLICIT SERIES OF $f(\eta)$

In this appendix, the recurrence formulas for $b^k_{m,n}$ in Eq. (45) are given. The coefficients of $f(\eta)$ read

$$b^0_{0,0} = -\frac{1}{\lambda}, \quad b^1_{0,0} = \frac{1}{\lambda}, \quad b^0_{0,1} = \frac{1}{\lambda}, \tag{A1}$$

and for $m \ge 1$, $0 \le n \le m+1$, and $0 \le k \le 2(m-n+1)$,

$$b^0_{m,0} = \chi_m\, b^0_{m-1,0} - \sum_{q=0}^{2m-1} \Gamma^q_{m,1}\mu^q_{1,1} - \sum_{n=2}^{m+1}\left[(n-1)\Gamma^0_{m,n}\mu^0_{n,0} + \sum_{q=1}^{2(m-n+1)} \Gamma^q_{m,n}(n\,\mu^q_{n,0} - \mu^q_{n,0} - \mu^q_{n,1})\right], \tag{A2}$$

$$b^1_{m,0} = 0, \tag{A3}$$

$$b^0_{m,1} = \chi_m b^0_{m-1,1} + \sum_{q=0}^{2m-1} \Gamma^q_{m,1}\mu^q_{1,1} + \sum_{n=2}^{m+1}\left[n\Gamma^0_{m,n}\mu^0_{n,0} + \sum_{q=1}^{2(m-n+1)} \Gamma^q_{m,n}(n\mu^q_{n,0} - \mu^q_{n,1})\right], \tag{A4}$$

$$b^k_{m,1} = \chi_m\, b^k_{m-1,1} + \sum_{q=k-1}^{2m-1} \Gamma^q_{m,1}\mu^q_{1,k}, \quad 1 \le k \le 2m-2, \tag{A5}$$

Published under an exclusive license by AIP Publishing

$$b^k_{m,1} = \sum_{q=k-1}^{2m-1} \Gamma^q_{m,1}\mu^q_{1,k}, \quad 2m-1 \le k \le 2m, \tag{A6}$$

$$b^k_{m,n} = \chi_m\, b^k_{m-1,n} - \sum_{q=k}^{2(m-n+1)} \Gamma^q_{m,n}\mu^q_{n,k}, \quad 0 \le k \le 2(m-n), \quad 2 \le n \le m, \tag{A7}$$

$$b^k_{m,n} = -\sum_{q=k}^{2(m-n+1)} \Gamma^q_{m,n}\mu^q_{n,k}, \quad 2(m-n)+1 \le k \le 2(m-n)+2, \quad 2 \le n \le m, \tag{A8}$$

$$b^0_{m,m+1} = -\Gamma^0_{m,m+1}\mu^0_{m+1,0}, \quad n = m+1, \tag{A9}$$

in which $\Gamma^q_{m,n}$ is defined by

$$\Gamma^q_{m,1} = c_0(C\lambda\hat{d}^q_{m-1,1} + \delta^q_{m,1}),\ 0 \le q \le 2m-2, \tag{A10}$$

$$\Gamma^{2m-1}_{m,1} = c_0\delta^{2m-1}_{m,1}, \tag{A11}$$

$$\Gamma^0_{m,m+1} = c_0\delta^0_{m,m+1}, \tag{A12}$$

$$\Gamma^q_{m,n} = c_0(C\lambda\hat{d}^q_{m-1,n} + \delta^q_{m,n}), \quad 0 \le q \le 2(m-n), \tag{A13}$$

$$\Gamma^q_{m,n} = c_0\delta^q_{m,n}, \quad 2(m-n)+1 \le q \le 2(m-n)+2, \tag{A14}$$

$$\Gamma^q_{m,n} = 0, \text{ otherwise}, \tag{A15}$$

where

$$\hat{d}^0_{m,m+1} = -(m+1)^3 b^0_{m,m+1}, \tag{A16}$$

$$\hat{d}^I_{m,k} = (i+1)c^{i+1}_{m,k} - kc^i_{m,k}, \quad 0 \le i \le 2(m-k)+1, \quad 1 \le k \le m, \tag{A17}$$

$$\hat{d}^i_{m,k} = -kc^i_{m,k}, \quad i = 2(m-k+1).\ 1 \le k \le m, \tag{A18}$$

in which

$$c^0_{m,m+1} = (m+1)^2 b^0_{m,m+1}, \tag{A19}$$

$$c^i_{m,k} = (i+1)(i+2)b^{i+2}_{m,k} - 2k(i+1)b^{i+1}_{m,k} + k^2 b^i_{m,k}, \quad 0 \le i \le 2(m-k), \quad 1 \le k \le m, \tag{A20}$$

$$c^i_{m,k} = -2k(i+1)b^{i+1}_{m,k} + k^2 b^i_{m,k}, \quad i = 2(m-k)+1, \quad 1 \le k \le m, \tag{A21}$$

$$c^i_{m,k} = k^2 b^i_{m,k}, \quad i = 2(m-k)+2, \quad 1 \le k \le m. \tag{A22}$$

For $1 \le n \le m+1$, $0 \le q \le 2(m-n+1)$,

$$\delta^q_{m,n} = \sum_{k=0}^{m-1}\sum_{j=J_0}^{J_1}\sum_{i=I_0}^{I_1} c^i_{k,j}\,\beta^{q-i}_{m-1-k,n-j} b^{q-i}_{m-1-k,n-j},$$
$$J_0 = max\{1, n+k-m\},$$
$$J_1 = min\{n, k+1\},$$
$$I_0 = max\{0, q-2(m-k-n+j)\},$$
$$I_1 = min\{q, 2(k-j+1)\}. \tag{A23}$$

Note that $\delta^{2m}_{m,1} = 0$ for $m \ge 1$, and $\beta^i_{m,k}$ in Eq. (A23) are given by

$$\beta^i_{m,k} = \begin{cases} 0, & m = k = 0,\ i \ge 2, \\ 0, & m > 0,\ k = 0,\ i \ge 1, \\ 0, & k > m+1, \\ 0, & i > 2(m+1-k), \\ 1, & \text{otherwise}. \end{cases} \tag{A24}$$

The parameter $\mu^q_{n,k}$ in Eqs. (A2)–(A9) is defined by

$$\mu^q_{1,k} = \frac{q!\,(2-k+q)}{k!}, \quad 0 \le k \le q+1, \quad q \ge 0, \tag{A25}$$

$$\mu^q_{n,k} = \frac{q!}{k!}\sum_{j=k}^{q}\frac{(j-k+1)}{(n-1)^{q-j+1}}\frac{1}{n^{j-k+2}} = \frac{q!}{k!}\frac{1}{(n-1)^{q-j+1}} \times \left\{1 - \left(1-\frac{1}{n}\right)^{q-k+1} \times \left[1 + (q-k+1)\frac{1}{n}\right]\right\}, \tag{A26}$$

for $0 \le k \le q$, $n \ge 2$, and $q \ge 0$.

APPENDIX B: COEFFICIENTS OF THE EXPLICIT SERIES OF $g(\eta)$

On the basis of Appendix A, the coefficients for the explicit and analytic expression of $g(\eta)$ are now presented in detail. The coefficients of $g(\eta)$ read

$$d^0_{0,0} = 1, \quad d^0_{0,1} = T^*_w - 1, \quad d^0_{m,0} = 0,\ m \ge 1, \tag{B1}$$

and for $m \ge 1$,

$$d^0_{m,1} = \chi_m d^0_{m-1,1} - \sum_{n=2}^{m}\left[\sum_{q=0}^{2(m-n)}\Pi^q_{m-1,n}w^q_{n,0} + \sum_{q=0}^{2(m+1-n)}\mathbb{K}^q_{m,n}w^q_{n,0} + \sum_{q=0}^{2(m-n+1)}\Omega^q_{m,n}w^q_{n,0}\right] - \left[\mathbb{K}^0_{m,m+1}w^0_{m+1,0} + \Omega^0_{m,m+1}w^0_{m+1,0}\right], \tag{B2}$$

$$d^l_{m,1} = \chi_m d^l_{m-1,1} + \left[\sum_{q=l}^{2m-1}\Pi^{q-1}_{m-1,1}w^{q-1}_{1,l} + \sum_{q=l}^{2m+1}\mathbb{K}^{q-1}_{m,1}w^{q-1}_{1,l}\right], \quad 1 \le l \le 2m-2, \tag{B3}$$

$$d^l_{m,1} = \sum_{q=l}^{2m-1}\Pi^{q-1}_{m-1,1}w^{q-1}_{1,l} + \sum_{q=l}^{2m+1}\mathbb{K}^{q-1}_{m,1}w^{q-1}_{1,l}, \quad l = 2m-1, \tag{B4}$$

$$d^l_{m,1} = \sum_{q=l}^{2m+1}\mathbb{K}^{q-1}_{m,1}w^{q-1}_{1,l}, \quad 2m \le l \le 2m+1, \tag{B5}$$

$$d^l_{m,n} = \chi_m d^l_{m-1,n} + \left[\sum_{q=l}^{2(m-n)}\Pi^q_{m-1,n}w^q_{n,l} + \sum_{q=l}^{2(m+1-n)}\mathbb{K}^q_{m,n}w^q_{n,l} + \sum_{q=l}^{2(m-n+1)}\Omega^q_{m,n}w^q_{n,l}\right], \quad 2 \le n \le m, \quad 0 \le l \le 2(m-n), \tag{B6}$$

$$d^l_{m,n} = \sum_{q=l}^{2(m+1-n)}\mathbb{K}^q_{m,n}w^q_{n,l} + \sum_{q=l}^{2(m-n+1)}\Omega^q_{m,n}w^q_{n,l}, \quad 2 \le n \le m, \quad 2(m-n)+1 \le l \le 2(m+1-n), \tag{B7}$$

Published under an exclusive license by AIP Publishing

$$d^0_{m,m+1} = \mathbb{K}^0_{m,m+1}\, w^0_{m+1,0} + \Omega^0_{m,m+1}\, w^0_{m+1,0}, \tag{B8}$$

in which $\Pi^q_{m-1,n}$, $\mathbb{K}^q_{m,n}$, $\Omega^q_{m,n}$, and $w^q_{n,l}$ are defined by

$$\Pi^q_{m-1,n} = c_0 C\lambda \varpi^q_{m-1,n}, \quad 1 \le n \le m, \quad 0 \le q \le 2(m-n), \tag{B9}$$

$$\mathbb{K}^q_{m,n} = c_0 Pr \kappa^q_{m,n}, \quad 1 \le n \le m+1, \quad 0 \le q \le 2(m+1-n), \tag{B10}$$

$$\Omega^q_{m,n} = c_0(\gamma-1)M_a^2 PrC\lambda^3 \sigma^q_{m,n}, \quad 2 \le n \le m+1, \quad 0 \le q \le 2(m+1-n), \tag{B11}$$

and

$$w^q_{1,i} = -\frac{q!}{i!}, \quad 0 \le i \le q+1, \quad q \ge 0, \tag{B12}$$

$$w^q_{n,i} = \frac{q!}{i!}\sum_{j=i}^{q}\frac{q!}{i!}\frac{1}{(n-1)^{q-j+1}}\frac{1}{n^{j-i+1}} = \frac{q!}{i!}\frac{1}{(n-1)^{q-i+1}}\left[1-\left(1-\frac{1}{n}\right)^{q-i+1}\right], \tag{B13}$$

for $n \ge 2$, $0 \le i \le q$, $q \ge 0$.

The related parameter $\varpi^i_{m,k}$ in Eq. (B9) is given by

$$\varpi^0_{m,m+1} = (m+1)^2 d^0_{m,m+1}, \tag{B14}$$

and for $1 \le k \le m$,

$$\varpi^i_{m,k} = (i+2)(i+1)d^{i+2}_{m,k} - 2k(i+1)d^{i+1}_{m,k} + k^2 d^i_{m,k}, \quad 0 \le i \le 2(m-k), \tag{B15}$$

$$\varpi^i_{m,k} = -2k(i+1)d^{i+1}_{m,k} + k^2 d^i_{m,k}, \quad i = 2(m-k)+1, \tag{B16}$$

$$\varpi^i_{m,k} = k^2 d^i_{m,k}, \quad i = 2(m-k+1). \tag{B17}$$

For $1 \le n \le m+1$, $0 \le q \le 2(m+1-n)$, the parameter $\kappa^i_{m,k}$ in Eq. (B10) reads

$$\kappa^q_{m,n} = \sum_{k=0}^{m-1}\sum_{j=J_0}^{J_1}\sum_{i=I_0}^{I_1}\tau^i_{k,j}\,\beta^{q-i}_{m-1-k,n-j}\,b^{q-i}_{m-1-k,n-j}, \tag{B18}$$

where J_0, J_1, I_0, and I_1 are defined by Eqs. (A23), and $\tau^i_{k,j}$ is as follows:

$$\tau^0_{m,m+1} = -(m+1)d^0_{m,m+1}, \tag{B19}$$

$$\tau^i_{m,k} = (i+1)d^{i+1}_{m,k} - kd^i_{m,k}, \quad 0 \le i \le 2(m-k)+1, \quad 1 \le k \le m, \tag{B20}$$

$$\tau^i_{m,k} = -kd^i_{m,k}, \; i = 2(m-k+1), \; 1 \le k \le m, \tag{B21}$$

and $\beta^i_{m,k}$ is defined by Eq. (A24).

For $2 \le n \le m+1$, $0 \le q \le 2(m-n+1)$, the parameter $\sigma^i_{m,k}$ in Eq. (B11) is given by

$$\sigma^q_{m,n} = \sum_{k=0}^{m-1}\sum_{j=\hat{J}_0}^{\hat{J}_1}\sum_{i=\hat{I}_0}^{\hat{I}_1} c^i_{k,j}\, c^{q-i}_{m-1-k,n-j}, \qquad \hat{J}_1 = min\{n-1, k+1\}, \tag{B22}$$

where J_0, I_0, and I_1 are defined by Eqs. (A23) and $c^i_{m,k}$ is defined by Eqs. (A19)–(A22).

REFERENCES

[1] F. A. Messiter, "Boundary-layer interaction theory," J. Appl. Mech. **50**, 1104 (1983).
[2] D. De Grazia, D. Moxey, S. J. Sherwin, M. A. Kravtsova, and A. I. Ruban, "Direct numerical simulation of a compressible boundary-layer flow past an isolated three-dimensional hump in a high-speed subsonic regime," Phys. Rev. Fluids **3**, 024101 (2018).
[3] D. Xu, J. Wang, M. Wan, C. Yu, X. Li, and S. Chen, "Effect of wall temperature on the kinetic energy transfer in a hypersonic turbulent boundary layer," J. Fluid Mech. **929**, A33 (2021).
[4] C. G. Hernández and X. Wu, "Receptivity of supersonic boundary layers over smooth and wavy surfaces to impinging slow acoustic waves," J. Fluid Mech. **872**, 849 (2019).
[5] M. Dong, Y. Liu, and X. S. Wu, "Receptivity of inviscid modes in supersonic boundary layers due to scattering of free-stream sound by localised wall roughness," J. Fluid Mech. **896**, A23 (2020).
[6] J. H. Ou and J. Chen, "Numerical study of supersonic boundary-layer modal stability for a slightly rarefied gas using Navier-Stokes approach," Phys. Fluids **33**, 114107 (2021).
[7] K. X. Zhu and X. S. Wu, "Effects of spanwise-periodic surface heating on supersonic boundary-layer instability," J. Fluid Mech. **940**, A20 (2022).
[8] M. Ugolotti, P. Orkwis, J. M. Oorebeek, H. Babinsky, and S. Duncan, "Experimental and computational investigations of a normal-hole-bled supersonic boundary layer," AAIA J. **53**, 3726–3736 (2015).
[9] H. H. Zong, Y. H. Luo, H. S. Yang, M. X. Tang, Y. Wu, and S. G. Guo, "Experimental investigation of supersonic boundary-layer tripping with a spanwise pulsed spark discharge array," J. Fluid Mech. **931**, A16 (2022).
[10] M. Yu and J. Luo, "Nonlinear interaction mechanisms of disturbances in supersonic flat-plate boundary layers," Sci. China: Phys., Mech. Astron. **57**, 2141 (2014).
[11] S. Semenov, "Numerical simulation of the sound waves interaction with a supersonic boundary layer," WSEAS Trans. Acoust. Music **4**, 21 (2017).
[12] T. Zhou, Y. Lu, Z. Liu, and C. Yan, "Direct numerical simulation of control of oblique breakdown in a supersonic boundary layer using a local cooling strip," Phys. Fluids **33**, 084101 (2021).
[13] Y. Liu, M. Dong, and X. Wu, "Generation of first Mack modes in supersonic boundary layers by slow acoustic waves interacting with streamwise isolated wall roughness," J. Fluid Mech. **888**, A10 (2020).
[14] H. Blasius, "Grenzschichten in flüssigkeiten mit kleiner reibung," Z. Angew. Math. Phys. **56**, 1–37 (1908).
[15] S. Liao, "The proposed homotopy analysis technique for the solution of nonlinear problems," Ph.D. thesis (Shanghai Jiao Tong University, Shanghai, 1992).
[16] S. Liao, *Beyond Perturbation: Introduction to the Homotopy Analysis Method* (Chapman and Hall/CRC, New York, 2003).
[17] S. Liao, "Notes on the homotopy analysis method: Some definitions and theorems," Commun. Nonlinear Sci. Numer. Simul. **14**, 983 (2009).
[18] S. Liao, *Homotopy Analysis Method in Nonlinear Differential Equations* (Springer-Verlag GmbH, Berlin/Heidelberg, 2012).
[19] J. K. Kevorkian and J. D. Cole, *Multiple Scale and Singular Perturbation Methods* (Springer, New York, 1996).
[20] R. H. Rand and D. Armbruster, *Perturbation Methods, Bifurcation Theory and Computer Algebra*, 1st ed. (Springer, 1987).
[21] M. Antonio, "Homotopy analysis method applied to electrohydrodynamic flow," Commun. Nonlinear Sci. Numer. Simul. **16**, 2730 (2011).
[22] C. J. Nassar, J. F. Revelli, and R. J. Bowman, "Application of the homotopy analysis method to the Poisson-Boltzmann equation for semiconductor devices," Commun. Nonlinear Sci. Numer. Simul. **16**, 2501 (2011).
[23] K. Vajravelu and R. A. Van Gorder, *Nonlinear Flow Phenomena and Homotopy Analysis: Fluid Flow and Heat Transfer* (Springer, 2012).
[24] X. Zhong and S. Liao, "Analytic approximations of Von Kármán plate under arbitrary uniform pressure-equations in integral form," Sci. China: Phys., Mech. Astron. **61**, 014611 (2018).
[25] Q. Yu, "Wavelet-based homotopy method for analysis of nonlinear bending of variable-thickness plate on elastic foundations," Thin-Walled Struct. **157**, 107105 (2020).
[26] J. Cheng, S. Zhu, and S. Liao, "An explicit series approximation to the optimal exercise boundary of American put options," Commun. Nonlinear Sci. Numer. Simul. **15**, 1148 (2010).

Published under an exclusive license by AIP Publishing

[27]J. Cheng and J. E. Zhang, "Analytical pricing of American options," Rev. Deriv. Res. **15**, 157 (2012).
[28]J. Sardanyés, C. Rodrigues, C. Januário, N. Martins, G. Gil-Gómez, and J. Duarte, "Activation of effector immune cells promotes tumor stochastic extinction: A homotopy analysis approach," Appl. Math. Comput. **252**, 484 (2015).
[29]D. Jorge, C. Januário, and N. Martins, "Explicit series solution for a glucose-induced electrical activity model of pancreatic beta-cells," Chaos, Solitons Fractals **76**, 1–9 (2015).
[30]S. Liao, "A new non-perturbative approach in quantum mechanics for time-independent Schrödinger equations," Sci. China: Phys., Mech. Astron. **63**, 234612 (2020).
[31]L. Liu, J. Rana, and S. Liao, "Analytical solutions for the hydrogen atom in plasmas with electric, magnetic, and Aharonov-Bohm flux fields," Phys. Rev. E **103**, 023206 (2021).
[32]A. Kimiaeifar, E. Lund, O. Thomsen, and J. Sørensen, "Application of the homotopy analysis method to determine the analytical limit state functions and reliability index for large deflection of a cantilever beam subjected to static co-planar loading," Comput. Math. Appl. **62**, 4646 (2011).
[33]A. C. Cullen and S. R. Clarke, "A fast, spectrally accurate homotopy based numerical method for solving nonlinear differential equations," J. Comput. Phys. **385**, 106 (2019).
[34]S. Liao, "An explicit, totally analytic approximate solution for Blasius' viscous flow problems," Int. J. Nonlinear Mech. **34**, 759 (1999).
[35]D. Xu, Z. Lin, S. Liao, and M. Stiassnie, "On the steady-state fully resonant progressive waves in water of finite depth," J. Fluid Mech. **710**, 379 (2012).
[36]Z. Liu, J. L. Sun, D. Xie, and Z. L. Lin, "On the near resonances of collinear steady-state wave groups in finite water depth," Ocean Eng. **182**, 584 (2019).
[37]D. L. Xu and Z. Liu, "A study on nonlinear steady-state waves at resonance in water of finite depth by the amplitude-based homotopy analysis method," J. Hydrodyn. **32**, 888–900 (2020).
[38]S. Liao, D. Xu, and M. Stiassnie, "On the steady-state nearly resonant waves," J. Fluid Mech. **794**, 175 (2016).
[39]X. Yang, F. Dias, and S. Liao, "On the steady-state resonant acoustic-gravity waves," J. Fluid Mech. **849**, 111 (2018).
[40]X. Zhong and S. Liao, "On the limiting Stokes wave of extreme height in arbitrary water depth," J. Fluid Mech. **843**, 653 (2018).
[41]L. Massa and J. A. Schetz, "Hypersonic heat flux reconstruction with distributed temperature sensors," J. Thermophys. Heat Transfer **34**, 331 (2020).
[42]C. W. Jiang, P. X. Guo, Z. X. Gao, and C. H. Lee, "Sensitivity analysis on supersonic-boundary-layer stability subject to perturbation of flow parameters," Phys. Fluids **33**, 084111 (2021).
[43]J. D. Anderson, *Hypersonic and High Temperature Gas Dynamics*, 2nd ed. (McGraw-Hill, 2006).
[44]F. M. White, *Viscous Fluid Flow*, 3rd ed. (Osborne McGraw-Hill, 1991).
[45]E. R. Van Driest, "Investigation of laminar boundary layer in compressible fluids using the Crocco method," Report No. NACA TN 2597 (1952).
[46]J. Kierzenka and L. F. Shampine, "A BVP solver based on residual control and the Matlab PSE," ACM Trans. Math. Software **27**, 299 (2001).
[47]See L. Liu, J. Li, and S. J. Liao, https://lijing.sjtu.edu.cn/codes/liuling2022pof.zip for "Mathematica package for supersonic flat-plate boundary layer flows" (2022).

Published under an exclusive license by AIP Publishing